Hysteresis modeling of timber-based structural systems using a combined data and model-driven approach

Hysteresis modeling of timber-based structural systems using a combined data and model-driven approach

Angelo Aloisio[a,*], Marco Martino Rosso[b], Asif Iqbal[c], Massimo Fragiacomo[a]

[a] *Civil and Environmental Engineering Department, Università degli Studi dell'Aquila, L'Aquila, 67100, Italy*

[b] *Politecnico di Torino, DISEG, Dipartimento di Ingegneria Strutturale, Edile e Geotecnica, Corso Duca Degli Abruzzi, 24, Turin, 10128, Italy*

[c] *Department of Civil Engineering, University of Northern British Columbia, Prince George, Canada*

[d] *Department of Civil, Construction-Architectural and Environmental Engineering, Università degli Studi dell'Aquila, Via G. Gronchi, 18, L'Aquila, 67100, Abruzzo, Italy*

Abstract

This paper presents a novel computational approach to empirical hysteresis modelling applied to timber-based structures based on a combined data model-driven strategy. While the backbone curve is simulated using the experimental cyclic response based on a step-by-step optimization problem (data-driven approach), analytical functions describe the re-loading curves (model-driven approach). Empirical hysteresis models developed so far for timber structures are model-driven. However, the backbone curves can exhibit a highly irregular non-smooth trend, difficult to mirror using analytical formulations. The challenge in mirroring the experimental backbone using closed-form formulations has led to an extended set of parameters to be calibrated in existing literature models This paper presents a novel approach to the empirical hysteresis model, where the experimental data are directly involved, as a whole, in the model formulation. This model aims to be a possible trade-off between model complexity and accuracy. A reduced number of parameters needed to describe the re-loading paths is counterbalanced using an entire subset of the experimental data. The paper delivers the developed Matlab and Python codes for further implementation as a user-defined element within a Finite Element software.

Keywords: Hysteresis models; timber engineering; shear walls; pinching; Cross-Lam timber; light-frame timber.

1. Introduction

Empirical hysteresis modelling is a branch of structural engineering devoted to simulating structural systems' experimental cyclic response. Empirical hysteresis models lack mechanical interpretation, blindly matching the experimental data [1]. There are differential and non-differential approaches to empirical hysteresis models. The most used differential models belong to the so-called Bouc-Wen class [1–5]. They are based on a first-order differential equation, representing the evolution of the inelastic displacement response. After the first paper by Bouc [6], other researchers presented modifications and extensions of the Bouc-Wen model to simulate asymmetric hysteresis, degradation phenomena and pinching [7–11].

Non-differential models originate from a piece-wise definition of the hysteresis loop [12–16]. The main differences between non-differential models stand in adopting diverse analytical functions for each section of the loop and proper continuity conditions. Most of the research in structural engineering, chiefly directed on applications, does not deal with differential hysteresis models more evolved than the Bouc-Wen class ones and focalizes on non-differential formulations due to flaws and challenges in using these models [7, 17–19].

In the last two decades, timber engineering experienced significant advancement in the development of non-differential models, featured by some stability advantages to the differential ones: they are generally faster and less computationally demanding. The primary objective in using empirical hysteresis modelling rather than finite elements is to simulate extended structural arrangements with multiple connections [3, 19–23]. The finite element modelling of each connection, where most dissipation is confined, may lead to a high computational cost [24–29]. Therefore, the modelling of a real-case structural arrangement with multiple dissipation sources entails

*Corresponding author.
Email address: angelo.aloisio1@univaq.it (Angelo Aloisio)

impractical finite element simulations due to the time length of the analysis. The development of reliable hysteresis models represents a crucial issue to reduce the duration of simulations [30–33]. The main differences between non-differential models stand in the definition of the piece-wise functions. There is the model by Polensek and Laursen [34] based on linear functions, the trilinear model by Rinaldin et al. [35] and the SAWS Material Model (OpenSees) [36]. Conversely, the CUREE model [37], the evolutionary parameter hysteretic model (EPHM) [38] and others [39, 40] present nonlinear branches. Dolan [41, 42] developed a transcendental hysteresis model based on four exponential functions that define the hysteretic curves. For a concise literature review of empirical hysteresis models for timber-based structural systems, the reader can refer to [43].

So far, no scholar proposed a hybrid approach to hysteresis, where the experimental data, not just their optimum fitting, participate in the model definition. Interestingly, while the backbone curves of timber-based assemblies exhibit a non-regular progression, the re-loading and un-loading curves present a more smooth trend, see in Fig.1 the cyclic response of a Cross-Laminated Timber shear wall. The main challenge in hysteresis modelling is the calibration of the degradation parameters for an optimum fitting of the backbone curve. The number of parameters boosts if the backbone curve is so irregular that the scholar must use a piece-wise definition of each loading path. Therefore, the model may grow in complexity due to the difficulties in mirroring the irregular backbone (abrupt strength decay, wavy trend, e.g.). Several models achieve a good fitting of the maximum force, neglecting the matching between simulated and real force values at lower displacement [43]. The empirical hysteresis model's goal is to achieve an almost exact correspondence between experimental and numerical data. Still, the erratic nature of the backbone curve requires specific analytical functions depending on the particular system under investigation. Accordingly, in this paper, the authors propose a hybrid approach to hysteresis. The first-loading curves (backbone) do not descend from analytical

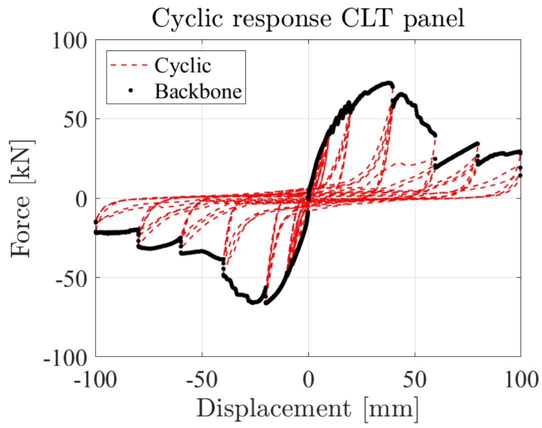

Figure 1: Experimental cyclic response of a Cross-Laminated Timber shear wall. The experimental tests are detailed in [44, 45].

functions but directly arise from a step-by-step optimization of the experimental backbone. Conversely, the re-loading and un-loading paths, exhibiting a smoother trend, have a straightforward definition based on power functions. The resulting hysteresis model could be advantageous to the reduced number of unknown parameters: the residual force at zero displacements and the exponents of the power functions. The authors observed that this model satisfactorily reproduces a set of experimental data expressing the variability of hysteresis on timber engineering. The calibration of the parameters is straightforward and does not require dedicated optimization. It can also originate from hand-tuning in practice-oriented circumstances due to their reduced variability and mutual correlation. The chief task in empirical hysteresis modelling can be to simulate the backbone curve: this issue is solved by directly adopting the experimental force values. The experimental data are always required for proper model calibration and are frequently available to the scholar who carries out structural analyses.

Therefore, the proposed formulation has two pieces of novelties compared to existing ones. (i) The inclusion of the experimental backbone, leading to a hybrid, analytical-numerical hysteresis model. (ii) Adopting the sole maximum displacement as an evolutionary parameter, ignoring the dependence on dissipated hysteretic energy.

The paper discusses the feasibility of a hybrid approach to empirical hysteresis modelling based on a data/model-driven strategy. The second section presents the mathematical formulation of the hysteresis model, while the third section addresses the fitting capacity of the model on a chosen dataset. The fourth section deals with the model validation using the experimental cyclic response of a given structure under different loading protocols. The last section gives concluding remarks about the current model development. The Appendix reports the complete MATLAB and Python codes developed by the authors for possible use by other researchers.

2. Hysteresis model formulation

The current hysteresis model originates from a heterogeneous formulation. The backbone curve, which delimits the upper and lower bounds of hysteresis, derives from an optimization problem based on the experimental cyclic response of the structural system. The re-loading and unloading curves are power functions whose coefficients derive from the fulfillment of the continuity conditions, while the exponent depending on the curvature of the experimental curves. Eq.(1) collects the experimental backbone:

$$\begin{aligned} \boldsymbol{d}^+ &= \{d_1^+, ..., d_i^+, ...d_n^+\} \\ \boldsymbol{f}^+ &= \{f_1^+, ..., f_i^+, ...f_n^+\} \\ \boldsymbol{d}^- &= \{d_1^-, ..., d_i^-, ...d_m^-\} \\ \boldsymbol{f}^- &= \{f_1^-, ..., f_i^-, ...f_m^-\} \end{aligned} \tag{1}$$

where d^+ and d^- are the positive and negative displacements associated to the positive $\boldsymbol{f}^+$ and negative $\boldsymbol{f}^-$ force values. Fig.2 illustrates the main idea behind the proposed formulation. The hysteresis loop consists of six different phases, identified by the sign of velocity, displacement, and the past displacement history. The authors did not include the force value in the definition of hysteresis to achieve a more stable transition between phases. The force value is unknown in displacement-driven simulations and cannot be swiftly included in the conditional statements defining the transition phases.

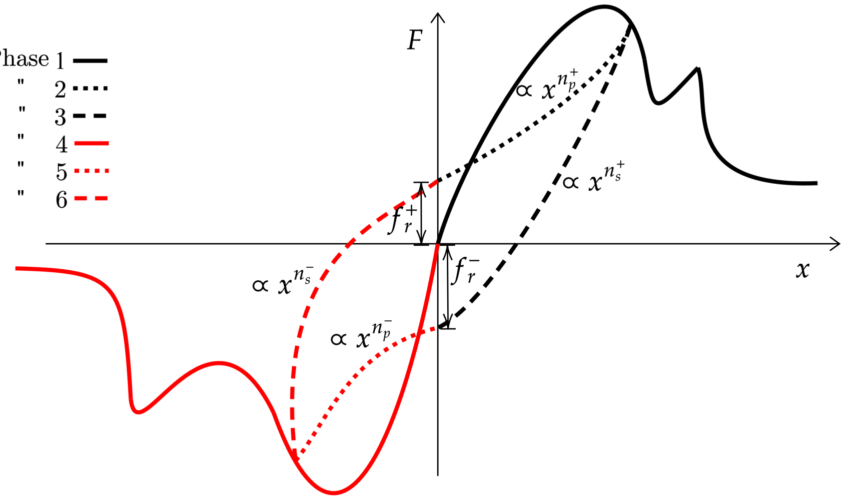

Figure 2: Definition of the hysteresis cycle based on the definition of six phases, identified by the sign of the displacement and velocity, and the occurring of pinching.

1. The first phase corresponds to the positive backbone, characterized by positive displacements, positive velocity and displacement higher than the maximum attained in the past history. The kth force value originates from the minimization of the squared difference between the kth simulated displacement x_k and the experimental displacement vector $\boldsymbol{d}^+$. The minimum argument of the resulting vector corresponds to the index of the optimum experimental force value, $\boldsymbol{f}^+$.
2. The second phase corresponds to the re-loading curve, characterized by positive displacements, positive velocity and displacement lower than the maximum attained in the past history. A power function with n_p^+ exponent defines the evolution of the resisting force. The coefficient is tuned to yield a force value corresponding to the maximum displacement attained in the past history. Accordingly, the stiffness of the pinching path depends on the maximum attained displacement. Therefore, the coefficient is variable and derives from step-by-step optimization similar to the one described in phase 1.
3. The third phase corresponds to the un-loading curve, characterized by positive displacements and negative velocity. A power function with n_s^+ exponent

defines the evolution of the resisting force. The coefficient is tuned to yield a force value corresponding to the maximum argument of the relative maximum displacement attained in the past history. Accordingly, the stiffness of this path depends on the fulfilment of the continuity between loading and unloading, imposing the identity of the force value. Therefore, the coefficient is variable and descends from step-by-step optimization based on the simulated data up to the kth integration step.

4. The fourth phase corresponds to the negative backbone, characterized by negative displacements, positive velocity and displacement lower than the maximum attained in the past history. The kth force value originates from the minimization of the squared difference between the kth simulated displacement x_k and the experimental displacement vector $\boldsymbol{d}^-$. The minimum argument of the resulting vector corresponds to the index of the optimum experimental force value, $\boldsymbol{f}^-$.

5. The fifth phase corresponds to the re-loading curve, characterized by negative displacements, positive velocity and displacement higher than the maximum attained in the past history. A power function with n_p^- exponent defines the evolution of the resisting force. The coefficient is tuned to yield a force value corresponding to the minimum displacement attained in the past history. Accordingly, the stiffness of the pinching path depends on the minimum attained displacement. Therefore, the coefficient is variable and derives from step-by-step optimization similar to the one described in phase 4.

6. The sixth phase corresponds to the un-loading curve, characterized by negative displacements and negative velocity. A power function with n_s^- exponent defines the evolution of the resisting force. The coefficient is tuned to yield a force value corresponding to the maximum argument of the relative minimum displacement attained in the past history. Accordingly, the stiffness of this path depends on the fulfilment of the continuity between loading and un-

loading, imposing the identity of the force value. Therefore, the coefficient is variable and descends from step-by-step optimization based on the simulated data up to the kth integration step.

The suggested hybrid formulation aims at reducing the number of unknown parameters by enhancing the model accuracy using the experimental cyclic response data. Eq.(2) collects into two vectors the input and output data. The input data are the positive and negative backbone values with additional six scalar parameters. The parameters can descend from a direct inspection of the experimental data or the solution of an optimization problem. Specifically, the n values identify the curvature of the power function, while f_r are the force values associated with zero displacements.

$$\begin{aligned} \text{Input} &= \{\boldsymbol{d}^+, \boldsymbol{d}^-, \boldsymbol{f}^+, \boldsymbol{f}^-, n_s^+, n_p^+, f_r^+, n_s^-, n_p^-, f_r^-\} \\ \text{Output} &= \{\boldsymbol{x}, \boldsymbol{f}\} \end{aligned} \tag{2}$$

The output data are the force and displacement vectors, $\boldsymbol{f}$ and $\boldsymbol{x}$ respectively. In displacement-driven simulations, the displacement is known and the outputs reduce to $\boldsymbol{f}$. Eq.(3) defines the displacement and force vectors up to the kth integration step, used in Eq.(4) for the formulation of the mathematical problem.

$$\begin{aligned} \boldsymbol{x}_k &= \{x_1, ..., x_k\} \\ \boldsymbol{f}_k &= \{f_1, ..., f_k\} \end{aligned} \tag{3}$$

Eq.(4), divided into six sections, represents the mathematical description of the proposed hysteresis model:

$$
\begin{aligned}
&\text{Phase 1}\\
&\text{if }\ \{x_k - x_{k-1} \geq 0,\ x_k \geq 0,\ x_k \geq \max(\boldsymbol{x}_k)\}\\
&f_k = \boldsymbol{f}^{+}(\arg\min_i (x_k - \boldsymbol{d}^{+})^2)\\
&-\\
&\text{Phase 2}\\
&\text{if }\ \{x_k - x_{k-1} \geq 0,\ x_k \geq 0,\ x_k < \max(\boldsymbol{x}_k)\}\\
&f_k = \tfrac{f_{\max} - f_r^{+}}{|\max(\boldsymbol{x}_k)|^{n_p^{+}}} |x_k|^{n_p^{+}} + f_r^{+}\\
&f_{\max} = \boldsymbol{f}^{+}(\arg\min_i (\max(\boldsymbol{x}_k) - \boldsymbol{d}^{+})^2)\\
&-\\
&\text{Phase 3}\\
&\text{if }\ \{x_k - x_{k-1} < 0,\ x_k \geq 0\\
&f_k = \tfrac{f_{\mathrm{m}} - f_r^{+}}{|x_{\mathrm{m}}|^{n_s^{+}}} |x_k|^{n_s^{+}} - f_r^{+}\\
&f_{\mathrm{m}} = f_{(\max(\mathrm{argmax}_k(\boldsymbol{\Delta f}_k)))} | \Delta f_k = f_k - f_{k-1}\\
&x_{\mathrm{m}} = x_{(\max(\mathrm{argmax}_k(\boldsymbol{\Delta x}_k)))} | \Delta x_k = x_k - x_{k-1}\\
&-\\
&\text{Phase 4}\\
&\text{if }\ \{x_k - x_{k-1} \geq 0,\ x_k < 0,\ x_k \leq \min(\boldsymbol{x}_k)\}\\
&f_k = \boldsymbol{f}^{-}(\arg\min_i (x_k - \boldsymbol{d}^{-})^2)\\
&-\\
&\text{Phase 5}\\
&\text{if }\ \{x_k - x_{k-1} \geq 0,\ x_k < 0,\ x_k > \min(\boldsymbol{x}_k)\}\\
&f_k = \tfrac{f_{\max} - f_r^{-}}{|\max(\boldsymbol{x}_k)|^{n_p^{-}}} |x_k|^{n_p^{-}} - f_r^{-}\\
&f_{\min} = \boldsymbol{f}^{-}(\arg\min_i (\min(\boldsymbol{x}_k) - \boldsymbol{d}^{-})^2)\\
&-\\
&\text{Phase 6}\\
&\text{if }\ \{x_k - x_{k-1} < 0,\ x_k < 0\\
&f_k = \tfrac{f_{\mathrm{l}} + f_r^{-}}{|x_{\mathrm{l}}|^{n_s^{-}}} |x_k|^{n_s^{-}} + f_r^{-}\\
&f_{\mathrm{l}} = f_{(\max(\arg\min_k(\boldsymbol{\Delta f}_k)))} | \Delta f_k = f_k - f_{k-1}\\
&x_{\mathrm{l}} = x_{(\max(\arg\min_k(\boldsymbol{\Delta x}_k)))} | \Delta x_k = x_k - x_{k-1}
\end{aligned}
\tag{4}
$$

The authors implemented the model in Eq.(4) in Matlab. The associated code is available to the scholar in the Appendix.

3. Results: response under imposed displacement

The authors estimated the fitting capacity of the proposed formulation with the experimental cyclic response of three structural systems: a Light-Timber Framed (LTF) and Cross-Laminated Timber (CLT) shear walls, and an angle bracket (AB). The three structural responses exhibited diverse distinctiveness and were chosen to estimate the performance of the proposed empirical hysteresis model. The dimension of the LTF shear wall is 2.5×2.5 m, see Fig.3(a). The test setup, shown in Fig.3(b), followed the EN 594:2011 protocol. The experimental data refer to a specimen with a vertical load equal to 20kN, two hold-downs, three angle brackets and an OBS sheathing fastened by nails to the framed structure. The frame elements are C24, with sections reported in Fig.3(a).

The CLT shear walls are 2.5×2.5 m, see Fig.4. They consist of three layers (thickness 30-30-30 mm) of C24 boards. The experimental data refer to a specimen with a vertical load equal to 20kN, two hold-downs and four angle brackets. The cyclic test data of three CLT shear walls, labelled STDL0-L0, NA620-L20 and NAWH-L20 after [45], have been used. The reader can refer to [44, 45] for additional details about the tested specimens and the experimental setup.

The Angle Bracket (AB) is a Reinforced Angle Bracket (105-R) - Simpson Strong-Tie 105mm × 105mm × 90mm. The experimental data refer to the shear response of the AB.

Figs.6,7,8 depict the comparison between the experimental and simulated data for the LTF, CLT and AB. The substantial symmetry of the experimental data determined the reduction of the unknown parameters from six to three. They are the residual force ($f_r = f_r^+ = f_r^-$) and the exponents of the power functions associated with the re-loading ($n_p = n_p^+ = n_p^-$) and un-loading paths ($n_s = n_s^+ = n_s^-$). The

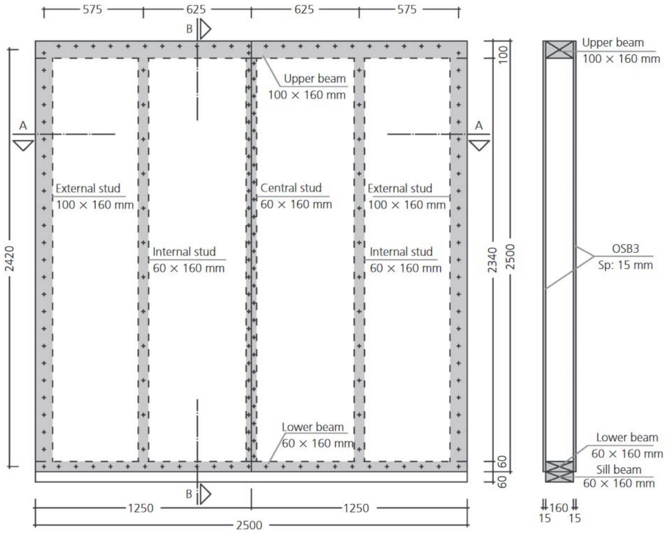

(a)

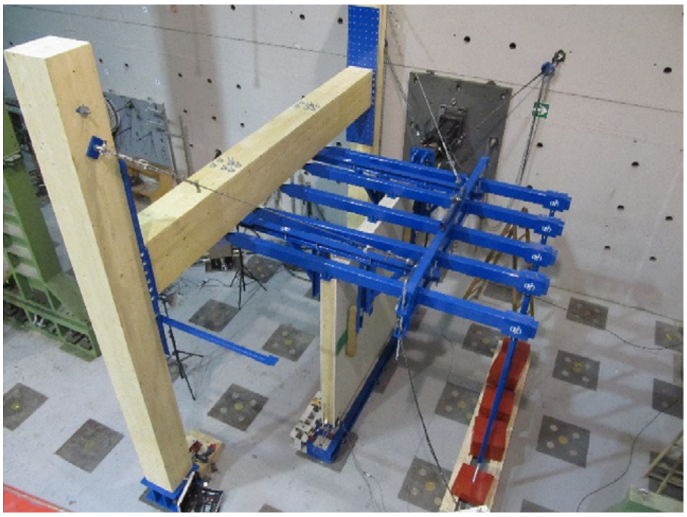

(b)

Figure 3: (a) Constructive details of the partially anchored LTF shear wall tested by [44, 45] and (b) a view of the experimental setup.

LTF manifests a progressive increment of the resisting force, the attainment of the maximum force close to 70kN and the force decaying at displacements higher than 30mm. The re-loading and un-loading curves have quite regular evolution up to 30mm, then the curve concavity changes in the last cycles. The n_p and n_s exponents are constant. Therefore, the least-square optimization of the unknown parameters led to a set of parameters closely following the experimental data up to 30mm. The pinching and un-loading paths of the last two cycles are associated with larger error due to n_p and n_s stationarity. Except for this inconsistency, the correspondence up

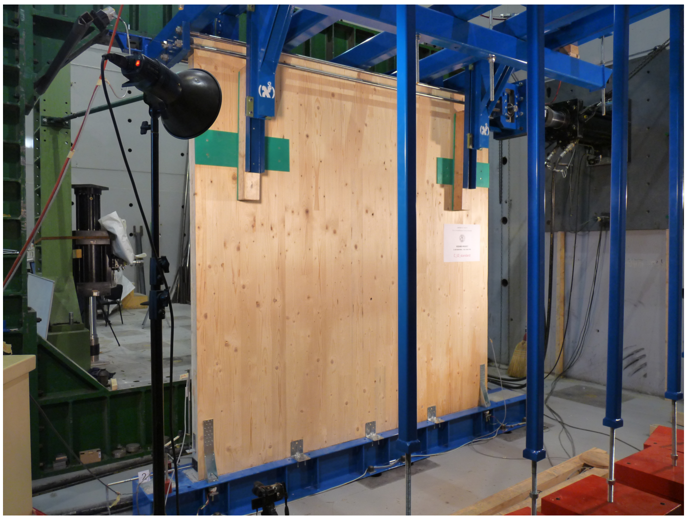

Figure 4: View of the CLT shear wall tested by [44, 45].

Figure 5: View of the angle bracket tested by the authors.

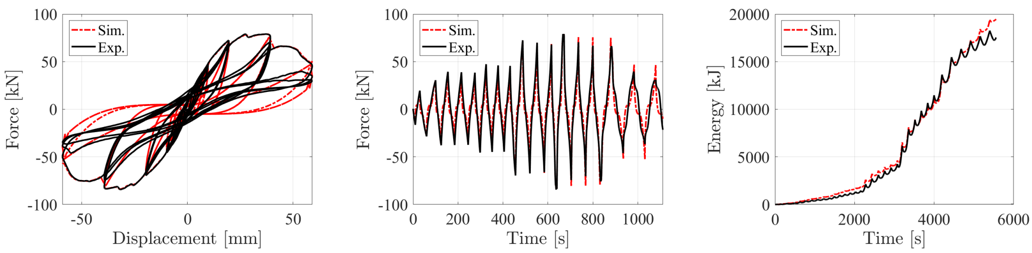

(a) (b) (c)

Figure 6: Comparison between the experimental cyclic response of a LTF shear wall and the proposed model in term of force-displacement (a), force-time (b) and energy-time (c) functions. Exp. stands for experimental data, while Sim. for simulated data.

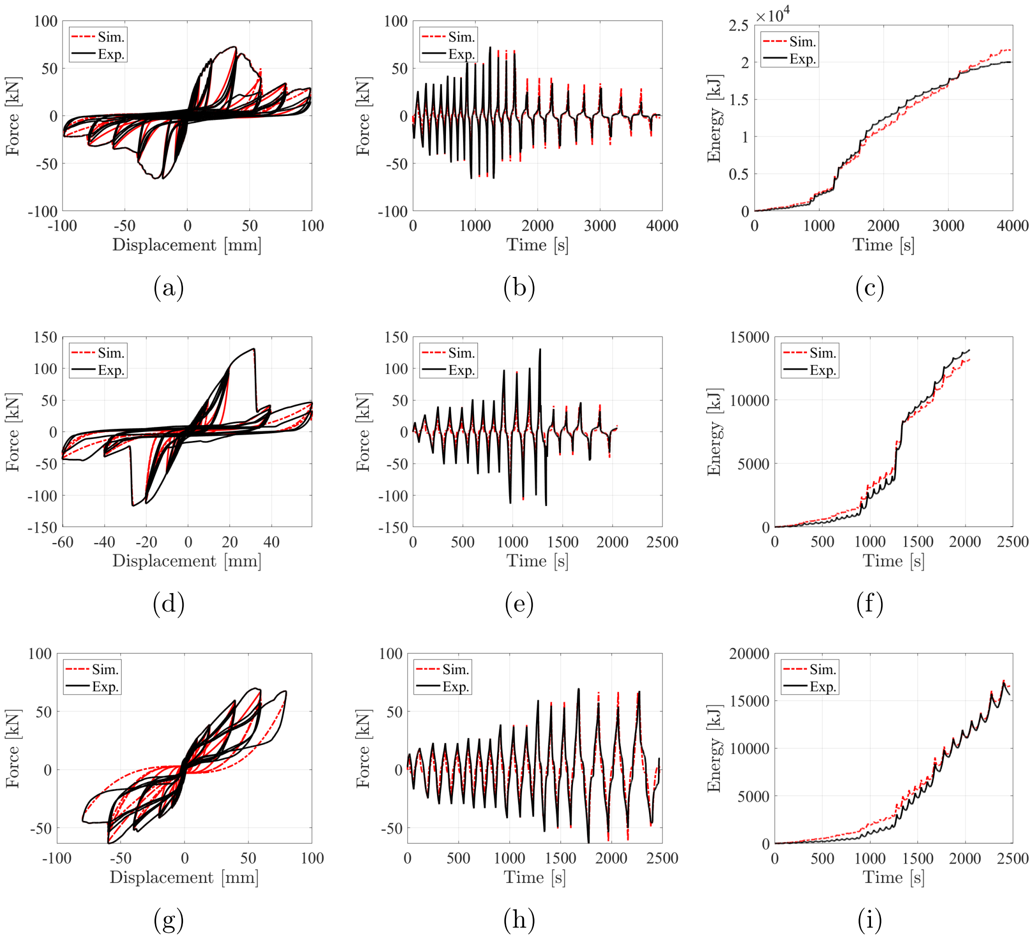

Figure 7: Comparison between the experimental cyclic response of three CLT shear walls (STDL0-L0 (a)-(c); NA620-L20 in (d)-(f); NAWH-L20 in (g)-(i), labelled after [45]) and the proposed model in term of force-displacement (a),(d), force-time (b),(e) and energy-time (c),(f) functions. Exp. stands for experimental data, while Sim. for simulated data.

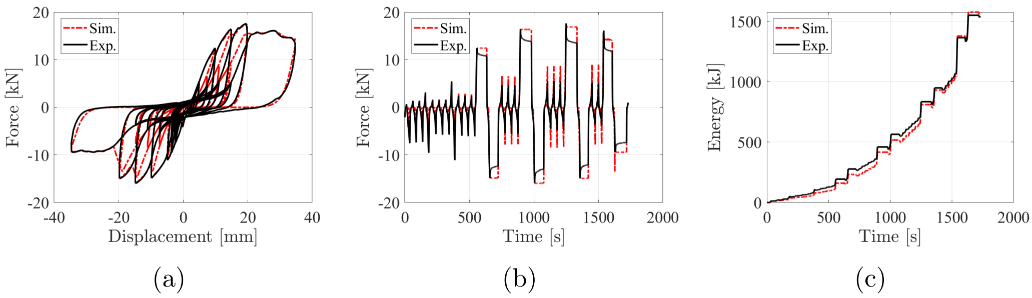

Figure 8: Comparison between the experimental cyclic response of an angle bracket and the proposed model, in term of force-displacement (a), force-time (b) and energy-time (c) functions. Exp. stands for experimental data, while Sim. for simulated data.

to 30mm is so accurate that it is difficult to distinguish the two superposed curves. The backbone of CLT is more erratic, as evidenced from Fig.1. There is a steady increment of the residual force, followed by an immediate decay due to the hold-down failure. After the abrupt force decrement, the force upholds at a lower value. In this circumstance, the re-loading and un-loading paths do not modify concavity, and constant values of n_p and n_s yield a reliable matching.

The cyclic response of the angle bracket is also peculiar due to the notable difference in the concavity of re-loading and un-loading. Still, this aspect is not an obstacle for the presented formulation. A significant difference between the two n_p and ns exponents mirrors the gap in the concavity. Interestingly, stationary parameters, like n_p and n_s, faithfully seize the variability of re-loading and unloading.

Table 1: Model parameters, Root Mean Square error (rmse) and maximum error corresponding to the models in Figs.6,7,8. The error is the difference between the experimental and simulated force vectors. The three values for the CLT panel refer to the three specimens STD-L0, NA620-L20 and NAWH-L20 labelled after [45].

Value	LTF	CLT	AB
$n_p^+ = n_p^-$	2.3	{3.5,3.1,1.5}	2.2
$n_s^+ = n_s^-$	4.2	{6.1,8.7,4.2}	13.9
$f_r^+ = f_r^-$ [kN]	5.11	{2.5,2.5,3.1}	2.1
Max error [kN]	37.34	{34.34, 45.47,43.21}	7.93
RMSE [kN]	9.7	{12.43, 20.12, 19.21}	1.37

Tab.1 shows the calibrated parameters of the three models, LTF CLT and AB, obtained from a Least-Squares Optimization. The residual forces do not exhibit substantial scatter and do not exceed the 10% of the maximum force. This aspect is characteristic of timber-based structures and highlights the limited significance of the residual force compared to other structural systems (rubber isolators, e.g.), where the role of f_r is determinant being very close to the maximum force. The exponents express the concavity of re-loading and un-loading. The difference between n_p and n_s leads to energy dissipation, corresponding to the area enclosed by the two paths. In the three structural systems, the n_p exponent almost stands between 2 and 3. Conversely, the n_s exponent has a higher variability and represents a key parameter affecting the differences in energy dissipation. It is approximately 4 in

LTF, 6 in CLT and boosts to 13.9 in AB.

Tab.1 also presents the Maximum Error (ME), which is the maximum difference between the simulated and experimental force values, and the Root Mean Square Error (RMSE). The RMS is always lower than the ME. It confirms that the model is, on average, quite corresponding to the experimental data. Nevertheless, in a few situations, the model strives to grasp the maximum force value due to nonstationary pinching fractions. It may occur the ratio between the force in the backbone and pinching path given a certain displacement is not constant. This occurrence can lead to an error in the estimate of the peak force.

Fig.6,7,8 and Tab.1 proved that there is a good correspondence between the experimental and simulated data. Still, the main limitations stand in the stationarity of the model parameters. Reasonably, the n exponents, the residual forces f_r and the pinching fractions are not constant but dependent on the displacement history. A higher matching can be achieved by selecting time-variant parameters. However, the model represents a compromise between the adoption of limited parameters and the model accuracy. The authors believe that despite the reduced number of parameters, the model expresses a satisfactory level of accuracy for engineering purposes.

Interestingly, the authors describe a degrading system with such limited parameters by including the experimental backbone within the formulation. Many scholars presented hysteresis models with pinching and degradation with many parameters [3]. The parameters must express both the shape of hysteresis and the dependence on the dissipated hysteretic energy. The dissipated hysteretic energy is the most used parameter for the simulation of time-variant systems. The last section discusses the role of dissipated energy in empirical hysteresis models.

The model displays a stable performance under non-stationary inputs (earthquake, e.g.) when the displacement vector is unknown and descends from the solution of a second-order nonlinear differential equation. The authors examine the model performance by modelling the structural response of the LTF archetype as Single-Degree-Of-Freedom (SDOF) systems. The following nonlinear ordinary differential equation describes the cyclic response of the LTF shear wall modelled as a SDOF system. The model has a lumped mass by the top, while the resisting force is the defined hysteresis model. The explicit fourth-order Runge–Kutta method is used for the temporal discretization of Eq's approximate solution (5).

$$m\ddot{x} + f_s = -m\ddot{x}_g \tag{5}$$

where m is the mass, x the displacement, $\ddot{x}$ the double derivative of x with respect to time, f_s the resisting inelastic force, and $\ddot{x}_g$ the ground acceleration. In the considered SDOF system, the mass $m = 1ton$.

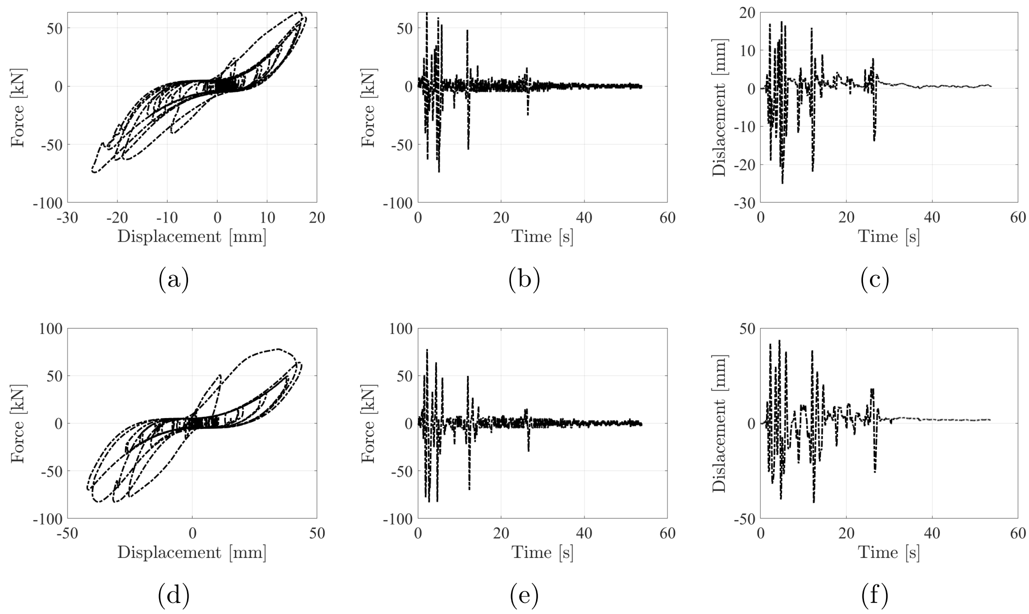

Figure 9: Integration of Eq.5 under El Centro earthquake with m=10ton, where the resisting force is the LTF model depicted in Fig.6. Plot of the force-displacement (a)-(d), force-time (b)-(e) and displacement-time (c)-(f) functions. (a)-(c) refer to the scaled El Centro earthquake multiplied by 0.5, while (d)-(f) to the unscaled earthquake (peak ground acceleration 0.349 g).

Fig.9 shows the response of the LTF system in Fig.6 under the El Centro earthquake. Fig.9(a)-(c) refers to the response under the El Centro earthquake uniformly scaled by a 0.5 factor. Fig.9(d)-(e) reveal the response of the same system under the unscaled earthquake. As anticipated, the system's response is very stable: the upper and lower bounds are the experimental backbone. Both simulations manifest the occurrence of pinching. However, the second is associated with a higher displacement due to the exceeding of 30mm displacement. The stability of empirical hysteresis models is essential and represents a crucial feature in evaluating its performance. Differential hysteresis models are more prone to exhibit unstable responses than non-differential ones [43]. Additionally, several hysteresis models do not manifest pinching under earthquake excitation. This result depends on the use of the dissipated energy as a time-dependent parameter. The weaknesses related to the use of the dissipated hysteretic energy are discussed in the following sections. In conclusion, the proposed model presents a stable performance and can simulate the structural response under pseudo-static and dynamic excitation.

4. Validation

This section deals with model validation. Firstly, the authors calibrate the model on the experimental cyclic response of a given structural system. Then, the response of the already calibrated model is compared to the experimental response of the same structural system excited by a different input. Precisely, the authors used the experimental cyclic response of plywood-coupled LVL wall panels detailed in [46]. Iqbal et al. investigated the response of the same plywood-coupled LVL wall to pseudo-static and pseudo-dynamic loading. The loading protocol adopted for pseudo-static symmetric cyclic testing was a modification of ACI T1.1-01, ACI T1.1R-01 [47], proposed for the testing on innovative jointed precast concrete frame systems.

Fig.10 presents the comparison between the experimental cyclic response of the prestressed plywood-coupled LVL shear wall and the calibrated hysteresis model. The shape of this system is also peculiar, characterized by more significant energy

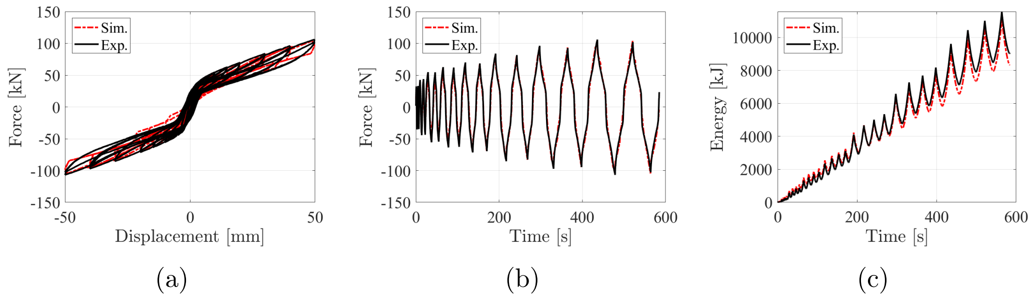

Figure 10: Comparison between the experimental cyclic response of a prestressed plywood-coupled LVL shear wall and the proposed model in term of force-displacement (a), force-time (b) and energy-time (c) functions. Exp. stands for experimental data, while Sim. for simulated data. Iqbal et al. provide full detail of the experimental setup in [46].

dissipation after the attainment of a displacement threshold. Accurately, a displacement approximately equal to 30mm is associated with a sudden stiffness decrement. The backbone resembles a sort of bi-linear function. However, the inclusion of the experimental data within the formulation does not entail an ad hoc definition of the first-loading path. The matching between the experimental and simulated response is very satisfactory, as proved by the force-time and energy-time functions in Fig.10(b)-(c). Tab.2 reports the optimized parameters and the associated error, comparable to the precedent cases.

Table 2: Model parameters, Root Mean Square error (rmse) and maximum error corresponding to the models in Figs.10,11. The error is the difference between the experimental and simulated force vectors.

Value	LVL pseudostatic	LVL pseudodynamic
$n_p^+ = n_p^-$	0.48	0.48
$n_s^+ = n_s^-$	0.81	0.81
$f_r^+ = f_r^-$ [kN]	10.3	10.3
Max error [kN]	33.6	35.63
RMSE [kN]	6.26	8.22

Fig.11 bestows the response of the real structural and the hybrid hysteresis model to pseudo-dynamic loading. The hysteresis model has been already calibrated, and the comparison between the two responses is a validation of the model: the scholar can theoretically use the model to extrapolate information using different inputs or, more generally, different structural configurations. Tab.2 proves that the error associated with the pseudo-dynamic tests is not much higher than the one associated

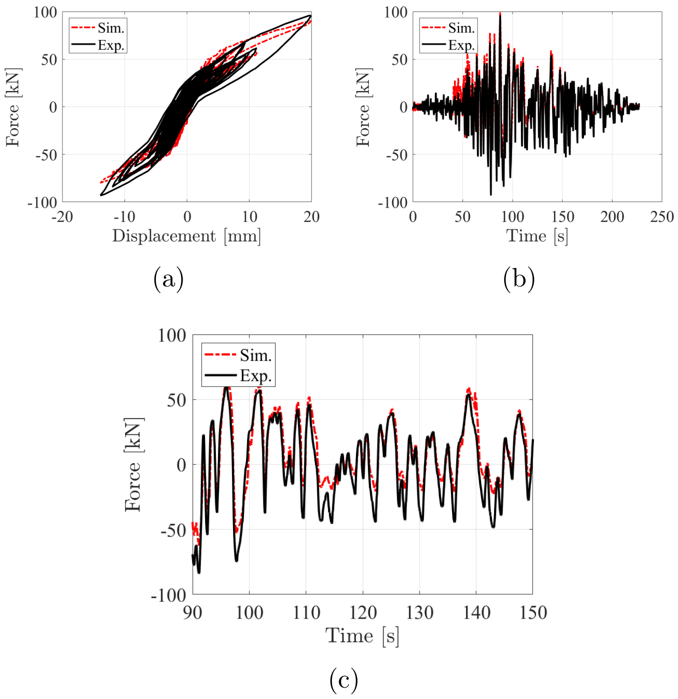

Figure 11: Comparison between the response of a prestressed plywood-coupled LVL shear wall and the proposed hybrid model under pseudo-dynamic tests in term of force-displacement (a), force-time (b) functions. Exp. stands for experimental data, while Sim. for simulated data; (c) is a detail of the force-time function in the central part of the plot in (b).

with the pseudo-static test. The model satisfactorily reproduces experimental data from cyclic tests, Fig.11. Consequently, experimental data could be considered adequately fitted for engineering purposes. In particular, the two responses are nearly coinciding in the central part of the graph, as evidenced in Fig.11(c).

5. Discussion: the role of the dissipated hysteretic energy

The proposed formulation has two pieces of novelties compared to existing ones. (i) The inclusion of the experimental backbone, leading to a hybrid, analytical-numerical hysteresis model. (ii) Adopting the sole maximum displacement as an evolutionary parameter, ignoring the dependence on dissipated hysteretic energy, often included in hysteresis models with degradation and pinching. Including the dissipated hysteretic energy can be valuable in certain circumstances, especially when the first-loading and re-loading paths have the same curvature sign [48]. However, in some instances, it can lead to inconsistent results. The following paragraphs attempt to explain the shortcomings possibly related to the use of the dissipated energy. In several formulations, like [3], the stiffness of the pinching path has the following exponential unfolding:

$$k_p \propto \exp(-\lambda\epsilon) \tag{6}$$

where λ is a coefficient and ϵ the dissipated hysteretic energy. The dissipated energy up to a given displacement value $\hat{d}$, corresponding to the kth integration step is:

$$\epsilon_k = \epsilon(\boldsymbol{d}_k) \tag{7}$$

where $\boldsymbol{d}_k$ collects the simulated displacement. Therefore, if the experimenter uses different loading protocols $\boldsymbol{d}_{k,1} \neq \boldsymbol{d}_{k,2}$, the resulting dissipated energy $\epsilon_k(\boldsymbol{d}_{k,1}) \neq \epsilon_k(\boldsymbol{d}_{k,2})$ can be different given a certain displacement value $\hat{d}$. Suppose the scholar calibrates the hysteresis model on experimental data characterized by a given displacement protocol $\boldsymbol{d}_1$. Then, the slope of the pinching path associated with a $\hat{d}$ displacement is labeled $k_{p,1}$. However, if he estimates the model response using a displacement protocol different from the one used for calibration ($\boldsymbol{d}_2$), the slope of the pinching path associated with the same $\hat{d}$, $k_{p,2}$ can be different than $k_{p,1}$, specifically $k_{p,1} \neq k_{p,2}$. If $\boldsymbol{d}_2$ leads to a lower dissipated energy when $d_k = \hat{d}$, the estimate of the pinching slope is biased. Accurately, the adoption of a displacement protocol yielding a lower dissipation in $\hat{d}$ leads to:

$$\hat{k}_{p,2} > \hat{k}_{p,1} \tag{8}$$

where $\hat{k}_{p,1}$ is the estimated stiffness based on the displacement protocol used for calibration ($\boldsymbol{d}_1$), while $\hat{k}_{p,1}$ is the estimated stiffness using a loading protocol ($\boldsymbol{d}_2$) associated with a lower dissipation in $\hat{d}$. The outgrowth of a biased stiffness estimate is an overestimation of the resisting force, surpassing the backbone curve. Fig.12

endeavours to illustrate this phenomenon. It shows two qualitative experimental cyclic responses of the same structural system. The first descends from the repetition of multiple cycles (solid black line), the second derives from the repetition of lower cycles (dashed red line). Reasonably, the slope of the pinching path can be different in the two experimental situations. However, the resisting force associated with a $\hat{d}$ displacement must be lower than the backbone in both cases. However, suppose the scholar adopts an exponential-like decaying of the stiffness depending on the dissipated energy. In that case, the slope of the pinching path obtained from a displacement $\boldsymbol{d}_2$ can be overestimated. The k_p overestimation leads to the exceeding of the backbone and inconsistent results.

This elementary example proves that adopting hysteretic energy as an evolutionary parameter may lead to a paradox, the resisting force of the pinching paths surpasses the backbone.

Most of the existing empirical hysteresis models use energy-based formulations. However, this rudimentary analysis proves that the outcomes of these models may be inconsistent if the scholar adopts a displacement protocol different from the calibration one.

The pinching phenomenon mostly depends on damage accumulation, and the dissipated hysteretic energy is an acknowledged indicator of progressive damage. Some scholars, starting from the pioneering Bouc-Wen-Barber-Noori (BWBN) model [2], do not define pinching using the sole maximum displacement. They adopt an energy-based formulation, where the stiffness of the loading path depends on the dissipated energy [49–51]. This formulation successfully works if the first-loading and re-loading paths have the same curvature [52, 53]. If the structural system manifests a curvature opposition between first-loading and re-loading, see Fig.2, the results can be biased under different displacement protocols.

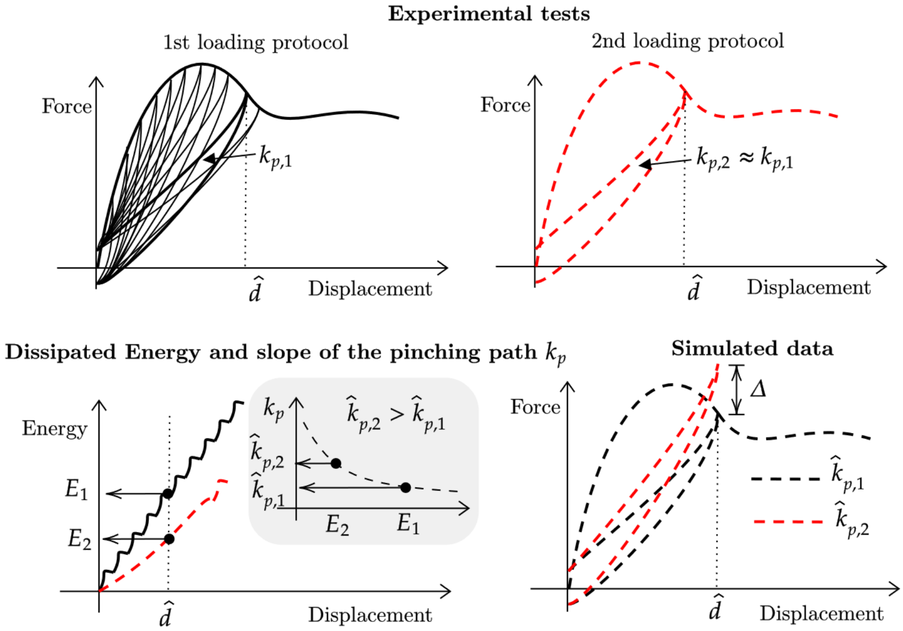

Figure 12: Illustration of the shortcomings possibly associated with energy-based formulations of degradation phenomena in empirical hysteresis models.

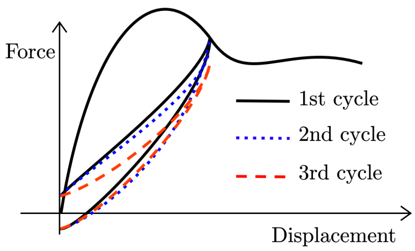

Figure 13: Effect of the dissipated hysteretic energy on multiple cycles.

Nevertheless, numerous experimental tests on different structural systems (reinforced concrete [54–57], timber [45, 58–61], masonry [62–65], e.g.) demonstrated that the slope of the pinching path chiefly depends on the maximum displacement rather than on the dissipated energy. Fig.13 attempts to explain the effect of dissipated hysteretic energy on multiple cycles. Specifically, the EN 594:2011 protocol includes the repetition of three cycles with the same amplitude. In most cases [66–74], what illustrated in Fig.13 appears. The repetition of the same cycle never yields force values higher than the backbone. The pinching and unloading paths slope can be different, possibly generating a lower force value (identified as a pinching fraction, q, [3]). However, the 2nd and 3rd cycles are very similar in most situations, like the ones displayed in Fig.6,7,8. Consequently, if the hysteresis model should have a limited number of parameters, the dissipated energy could be ignored. It yields minor effects compared to those associated with the maximum attained displacement. The current paper proves that a hysteresis model based on the sole definition of the maximum displacement can yield a satisfactory agreement with the experimental data for engineering purposes.

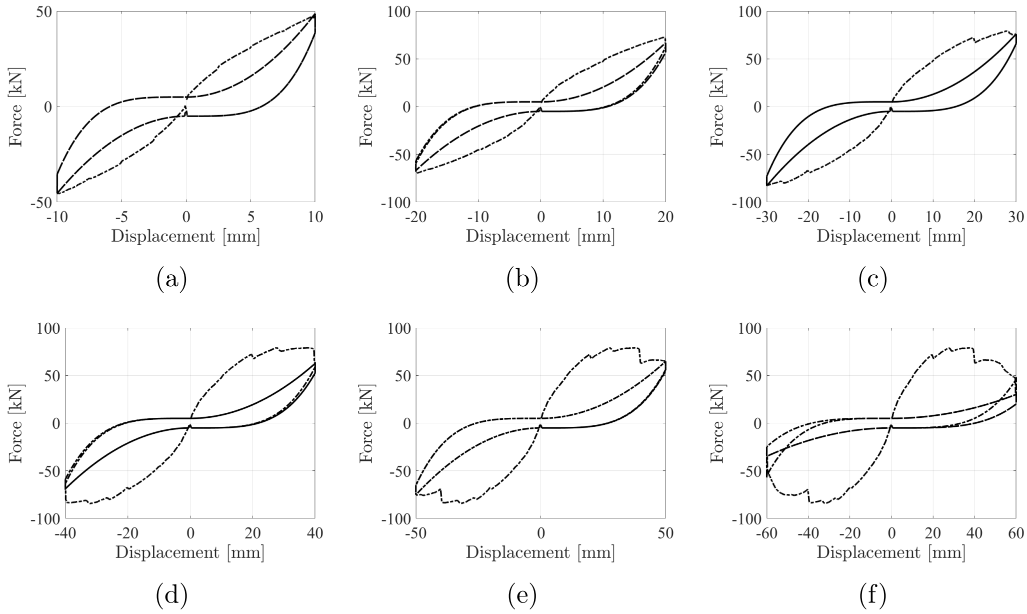

Figure 14: Cyclic response of of the LTF model in Fig.6 using sinusoidal imposed displacement with growing amplitude from (a) to (f).

Fig.14 shows the response of the LTF model under sinusoidal excitation, growing from 10 to 60mm. Fig.14 proves that the model return consistent results, upper bounded by the backbone, under displacement protocols different from the calibration ones.

6. Conclusions

The current paper presents an alternative way to empirical hysteresis modelling in structural engineering. The need for empirical hysteresis models originates from the necessity to estimate the inelastic response of complex structural arrangements without adopting a whole Finite Element approach. Finite Element analyses would entail time-consuming simulations, possibly impractical in working applications and some research activities. The authors propose a non-differential hysteresis model based on the partition of the hysteresis loop into six parts, distinguished by the signs of velocity and displacement and the past displacement history. The formulation has two significant pieces of novelties. (i) The first-loading paths originate from the experimental backbone by solving a step-by-step optimization problem. (ii) The evolution of degradation phenomena is driven by time-variant coefficients, where the sole maximum attained displacement and not the dissipated hysteretic energy determine the strength and stiffness evolution. This choice derives from possible weaknesses in using the dissipated hysteretic energy as a degradation parameter under input displacements different from the experimental ones. The proposed model is defined as a hybrid, being the product of an analytical formulation and the outcome of an optimization problem. The advantages in using this model stand in the limited number of unknown parameters, six, and the significant stability of time-integration under non-stationary inputs. The quality of a hysteresis model derives from balancing accuracy and the number of governing parameters. The best model should achieve a good correspondence with the lowest number of parameters. The authors proved the model versatility on three experimental cyclic responses. Then, they validated the model on the experimental response of a structural system under different displacement inputs. The model faithfully reproduces the experimental data and can represent a valid alternative to traditional empirical hysteresis models based on an entire analytical approach. The authors developed the model in Matlab. In the appendix, the reader can find the implemented code for displacement-driven simulations.

References

[1] A. Aloisio, R. Alaggio, J. Köhler, and M. Fragiacomo, "Extension of generalized bouc-wen hysteresis modeling of wood joints and structural systems," *Journal of Engineering Mechanics*, vol. 146, no. 3, p. 04020001, 2020.

[2] T. T. Baber and M. N. Noori, “Random vibration of degrading, pinching systems,” *Journal of Engineering Mechanics*, vol. 111, no. 8, pp. 1010–1026, 1985.

[3] G. C. Foliente, “Hysteresis modeling of wood joints and structural systems,” *Journal of Structural Engineering*, vol. 121, no. 6, pp. 1013–1022, 1995.

[4] J. Song and A. Der Kiureghian, “Generalized bouc–wen model for highly asymmetric hysteresis,” *Journal of engineering mechanics*, vol. 132, no. 6, pp. 610–618, 2006.

[5] S. Sirotti, M. Pelliciari, F. Di Trapani, B. Briseghella, G. Carlo Marano, C. Nuti, and A. M. Tarantino, “Development and validation of new bouc–wen data-driven hysteresis model for masonry infilled rc frames,” *Journal of Engineering Mechanics*, vol. 147, no. 11, p. 04021092, 2021.

[6] R. Bouc, “Solution periodique de lequation de la ferroresonance avec hysteresis,” *COMPTES RENDUS HEBDOMADAIRES DES SEANCES DE L ACADEMIE DES SCIENCES SERIE A*, vol. 263, no. 15, p. 497, 1966.

[7] M. Ismail, F. Ikhouane, and J. Rodellar, “The hysteresis bouc-wen model, a survey,” *Archives of Computational Methods in Engineering*, vol. 16, no. 2, pp. 161–188, 2009.

[8] W. Pu, C. Liu, and F. Dai, “Optimum hysteretic damper design for multi-story timber structures represented by an improved pinching model,” *Bulletin of Earthquake Engineering*, vol. 16, no. 12, pp. 6221–6241, 2018.

[9] A. Di Cesare, F. C. Ponzo, S. Pampanin, T. Smith, D. Nigro, and N. Lamarucciola, “Displacement based design of post-tensioned timber framed buildings with dissipative rocking mechanism,” *Soil Dynamics and Earthquake Engineering*, vol. 116, pp. 317–330, 2019.

[10] A. Aloisio, M. Pelliciari, A. V. Bergami, R. Alaggio, B. Briseghella, and M. Fragiacomo, “Effect of pinching on structural resilience: performance of reinforced concrete and timber structures under repeated cycles,” *Structure and Infrastructure Engineering*, pp. 1–17, 2022.

[11] A. Aloisio, M. Pelliciari, R. Alaggio, C. Nuti, M. Fragiacomo, and B. Briseghella, “Structural robustness of an rc pier under repeated earthquakes,” in *Proceedings of the Institution of Civil Engineers-Bridge Engineering*, pp. 1–20, Thomas Telford Ltd, 2021.

[12] W. Ramberg and W. R. Osgood, “Description of stress-strain curves by three parameters,” 1943.

[13] M. Menegotto, “Method of analysis for cyclically loaded rc plane frames including changes in geometry and non-elastic behavior of elements under combined normal force and bending,” in *Proc. of IABSE symposium on resistance and ultimate deformability of structures acted on by well defined repeated loads*, pp. 15–22, 1973.

[14] N. Vaiana, F. Marmo, S. Sessa, and L. Rosati, “Modeling of the hysteretic behavior of wire

rope isolators using a novel rate-independent model," in *Nonlinear Dynamics of Structures, Systems and Devices*, pp. 309–317, Springer, 2020.

[15] A. Pacitti, M. Peigney, F. Bourquin, and W. Lacarbonara, "Experimental data based cable tension identification via nonlinear static inverse problem," *Procedia engineering*, vol. 199, pp. 453–458, 2017.

[16] A. Tatar and D. M. Dowden, "Analytical and numerical investigation of a low-damage uplift friction damper for self-centering cross-laminated timber rocking walls," *Engineering Structures*, vol. 254, p. 113836, 2022.

[17] A. Aloisio, M. Pelliciari, S. Sirotti, F. Boggian, and R. Tomasi, "Optimization of the structural coupling between rc frames, clt shear walls and asymmetric friction connections," *Bulletin of Earthquake Engineering*, pp. 1–26, 2022.

[18] A. Aloisio, F. Boggian, and R. Tomasi, "Design of a novel seismic retrofitting system for rc structures based on asymmetric friction connections and clt panels," *Engineering Structures*, vol. 254, p. 113807, 2022.

[19] A. Aloisio, F. Boggian, R. Tomasi, and M. Fragiacomo, "Reliability-based assessment of ltf and clt shear walls under in-plane seismic loading using a modified bouc-wen hysteresis model," *ASCE-ASME Journal of Risk and Uncertainty in Engineering Systems, Part A: Civil Engineering*, vol. 7, no. 4, p. 04021065, 2021.

[20] B. Kivell, P. Moss, and A. Carr, "Hysteretic modelling of moment-resisting nailed timber joints," *Earthquake Engineering*, vol. 14, no. 4, 1981.

[21] D. Dowrick, "Hysteresis loops for timber structures," *Bulletin of the New Zealand Society for Earthquake Engineering*, vol. 19, no. 2, pp. 143–152, 1986.

[22] M. He, F. Lam, and R. O. Foschi, "Modeling three-dimensional timber light-frame buildings," *Journal of Structural Engineering*, vol. 127, no. 8, pp. 901–913, 2001.

[23] J.-Q. Yang, S. T. Smith, Z. Wang, P. Feng, and N. Sirach, "Modelling of hysteresis behaviour of moment-resisting timber joints strengthened with frp composites," *International Journal of Mechanical Sciences*, p. 105593, 2020.

[24] H. T. Nguyen and S. E. Kim, "Finite element modeling of push-out tests for large stud shear connectors," *Journal of Constructional Steel Research*, vol. 65, no. 10-11, pp. 1909–1920, 2009.

[25] T. Gečys, A. Daniūnas, T. K. Bader, L. Wagner, and J. Eberhardsteiner, "3d finite element analysis and experimental investigations of a new type of timber beam-to-beam connection," *Engineering structures*, vol. 86, pp. 134–145, 2015.

[26] A. Hassanieh, H. Valipour, M. Bradford, and C. Sandhaas, "Modelling of steel-timber composite connections: Validation of finite element model and parametric study," *Engineering*

Structures, vol. 138, pp. 35–49, 2017.

[27] C. Bedon and M. Fragiacomo, "Numerical analysis of timber-to-timber joints and composite beams with inclined self-tapping screws," *Composite Structures*, vol. 207, pp. 13–28, 2019.

[28] C. Bedon, G. Rinaldin, M. Fragiacomo, and S. Noé, "q-factor estimation for 3d log-house timber buildings via finite element analyses," *Soil Dynamics and Earthquake Engineering*, vol. 116, pp. 215–229, 2019.

[29] Y. De Santis and M. Fragiacomo, "Timber-to-timber and steel-to-timber screw connections: Derivation of the slip modulus via beam on elastic foundation model," *Engineering Structures*, vol. 244, p. 112798, 2021.

[30] J. Humbert, C. Boudaud, J. Baroth, S. Hameury, and L. Daudeville, "Joints and wood shear walls modelling i: Constitutive law, experimental tests and fe model under quasi-static loading," *Engineering Structures*, vol. 65, pp. 52–61, 2014.

[31] K. Vogrinec, M. Premrov, and E. K. Šilih, "Simplified modelling of timber-framed walls under lateral loads," *Engineering structures*, vol. 111, pp. 275–284, 2016.

[32] J. Jayamon, F. Charney, F. Flores, and P. Line, "Influence of wall load-displacement shape on seismic performance of wood-frame shear wall structures," in *World Conference on Timber Engineering*, 2016.

[33] Ö. Anil, A. Togay, Ü. K. Işleyen, N. Döngel, and C. Söğütlü, "Effect of timber type and nail spacing on the hysteretic behavior of timber-framed shear walls with openings," *International Journal of Civil Engineering*, vol. 16, no. 6, pp. 629–646, 2018.

[34] A. Polensek and H. I. Laursen, *Seismic Behavior of Bending Components and Intercomponent Connections of Light Frame Wood Buildings.* Oregon State University, 1984.

[35] G. Rinaldin, C. Amadio, and M. Fragiacomo, "A component approach for the hysteretic behaviour of connections in cross-laminated wooden structures," *Earthquake engineering & structural dynamics*, vol. 42, no. 13, pp. 2023–2042, 2013.

[36] G. Di Gangi, C. Demartino, G. Quaranta, and G. Monti, "Dissipation in sheathing-to-framing connections of light-frame timber shear walls under seismic loads," *Engineering Structures*, vol. 208, p. 110246, 2020.

[37] B. Folz and A. Filiatrault, "Seismic analysis of woodframe structures. i: Model formulation," *Journal of Structural Engineering*, vol. 130, no. 9, pp. 1353–1360, 2004.

[38] W. Pang, D. Rosowsky, S. Pei, and J. Van de Lindt, "Evolutionary parameter hysteretic model for wood shear walls," *Journal of structural engineering*, vol. 133, no. 8, pp. 1118–1129, 2007.

[39] J. P. Judd and F. S. Fonseca, "Analytical model for sheathing-to-framing connections in wood shear walls and diaphragms," *Journal of structural engineering*, vol. 131, no. 2, pp. 345–352,

2005.

[40] A. Blasetti, R. Hoffman, and D. Dinehart, “Simplified hysteretic finite-element model for wood and viscoelastic polymer connections for the dynamic analysis of shear walls,” *Journal of structural engineering*, vol. 134, no. 1, pp. 77–86, 2008.

[41] J. D. Dolan, *The dynamic response of timber shear walls.* PhD thesis, University of British Columbia, 1989.

[42] J. Xu and J. D. Dolan, “Development of nailed wood joint element in abaqus,” *Journal of structural engineering*, vol. 135, no. 8, pp. 968–976, 2009.

[43] A. Aloisio, P. Sejkot, A. Iqbal, and M. Fragiacomo, “An empirical transcendental hysteresis model for structural systems with pinching and degradation,” *Earthquake Engineering & Structural Dynamics*, 2021.

[44] P. Grossi, T. Sartori, and R. Tomasi, “Tests on timber frame walls under in-plane forces: part 2,” *Proceedings of the Institution of Civil Engineers-Structures and Buildings*, vol. 168, no. 11, pp. 840–852, 2015.

[45] A. Aloisio, F. Boggian, T. Roberto, and M. Fragiacomo, “The role of the hold-down in the capacity model of clt andltf shear walls based on the experimental lateral response,” *Construction and Building Materials*, vol. In press, 2021.

[46] A. Iqbal, M. Fragiacomo, S. Pampanin, and A. Buchanan, “Seismic resilience of plywood-coupled lvl wall panels,” *Engineering Structures*, vol. 167, pp. 750–759, 2018.

[47] A. I. T. G. 1, “Acceptance criteria for moment frames based on structural testing (t1. 1-01) and commentary (t1. 1r-01): An aci standard,” American Concrete Institute, 2001.

[48] M. Pelliciari, B. Briseghella, F. Tondolo, L. Veneziano, C. Nuti, R. Greco, D. Lavorato, and A. M. Tarantino, “A degrading bouc–wen model for the hysteresis of reinforced concrete structural elements,” *Structure and Infrastructure Engineering*, vol. 16, no. 7, pp. 917–930, 2020.

[49] G. A. Ortiz, D. A. Alvarez, and D. Bedoya-Ruíz, “Identification of bouc–wen type models using multi-objective optimization algorithms,” *Computers & Structures*, vol. 114, pp. 121–132, 2013.

[50] G. Peng, W. Li, H. Du, H. Deng, and G. Alici, “Modelling and identifying the parameters of a magneto-rheological damper with a force-lag phenomenon,” *Applied Mathematical Modelling*, vol. 38, no. 15-16, pp. 3763–3773, 2014.

[51] G. Marano, M. Pelliciari, T. Cuoghi, B. Briseghella, D. Lavorato, and A. Tarantino, “Degrading bouc–wen model parameters identification under cyclic load,” *International Journal of Geotechnical Earthquake Engineering (IJGEE)*, vol. 8, no. 2, pp. 60–81, 2017.

[52] A. Manzoori and H. Toopchi-Nezhad, "Application of an extended bouc-wen model in seismic response prediction of unbonded fiber-reinforced isolators," *Journal of Earthquake Engineering*, vol. 21, no. 1, pp. 87–104, 2017.

[53] V. Niola, G. Palli, S. Strano, and M. Terzo, "Nonlinear estimation of the bouc-wen model with parameter boundaries: Application to seismic isolators," *Computers & Structures*, vol. 222, pp. 1–9, 2019.

[54] F. Colangelo, "Pseudo-dynamic seismic response of reinforced concrete frames infilled with non-structural brick masonry," *Earthquake engineering & structural dynamics*, vol. 34, no. 10, pp. 1219–1241, 2005.

[55] A. B. Mehrabi, P. Benson Shing, M. P. Schuller, and J. L. Noland, "Experimental evaluation of masonry-infilled rc frames," *Journal of Structural engineering*, vol. 122, no. 3, pp. 228–237, 1996.

[56] L. Cavaleri and F. Di Trapani, "Cyclic response of masonry infilled rc frames: Experimental results and simplified modeling," *Soil Dynamics and Earthquake Engineering*, vol. 65, pp. 224–242, 2014.

[57] A. V. Bergami and C. Nuti, "Experimental tests and global modeling of masonry infilled frames," *Earthquakes and Structures*, vol. 9, no. 2, pp. 281–303, 2015.

[58] I. Gavric, M. Fragiacomo, and A. Ceccotti, "Cyclic behavior of clt wall systems: Experimental tests and analytical prediction models," *Journal of Structural Engineering*, vol. 141, no. 11, p. 04015034, 2015.

[59] J. Schneider, Y. Shen, S. Stiemer, and S. Tesfamariam, "Assessment and comparison of experimental and numerical model studies of cross-laminated timber mechanical connections under cyclic loading," *Construction and Building Materials*, vol. 77, pp. 197–212, 2015.

[60] R. Tomasi and T. Sartori, "Mechanical behaviour of connections between wood framed shear walls and foundations under monotonic and cyclic load," *Construction and Building Materials*, vol. 44, pp. 682–690, 2013.

[61] A. Aloisio, R. Alaggio, and M. Fragiacomo, "Equivalent viscous damping of cross-laminated timber structural archetypes," *Journal of Structural Engineering*, vol. 147, no. 4, p. 04021012, 2021.

[62] M. Angiolilli and A. Gregori, "Triplet test on rubble stone masonry: Numerical assessment of the shear mechanical parameters," *Buildings*, vol. 10, no. 3, p. 49, 2020.

[63] G. Vasconcelos and P. B. Lourenço, "In-plane experimental behavior of stone masonry walls under cyclic loading," *Journal of structural engineering*, vol. 135, no. 10, pp. 1269–1277, 2009.

[64] S. M. Nolph and M. A. ElGawady, "Static cyclic response of partially grouted masonry shear

walls," *Journal of structural engineering*, vol. 138, no. 7, pp. 864–879, 2012.

[65] D. Malomo, M. J. DeJong, and A. Penna, "Distinct element modelling of the in-plane cyclic response of urm walls subjected to shear-compression," *Earthquake Engineering & Structural Dynamics*, vol. 48, no. 12, pp. 1322–1344, 2019.

[66] Z. Li, X. Zheng, M. He, Y. Sun, and G. He, "Experimental and analytical investigations into the time-dependent performance in post-tensioned timber beam-column joints under sustained loads and varied environment," *Construction and Building Materials*, vol. 251, p. 118943, 2020.

[67] B. Shi, W. Zhu, H. Yang, W. Liu, H. Tao, and Z. Ling, "Experimental and theoretical investigation of prefabricated timber-concrete composite beams with and without prestress," *Engineering Structures*, vol. 204, p. 109901, 2020.

[68] H. Mpidi Bita and T. Tannert, "Experimental study of disproportionate collapse prevention mechanisms for mass-timber floor systems," *Journal of Structural Engineering*, vol. 146, no. 2, p. 04019199, 2020.

[69] S. Miller, J. E. Woods, J. Erochko, D. T. Lau, and C. F. Gilbert, "Experimental and analytical fragility assessment of a combined heavy timber–steel-braced frame through hybrid simulation," *Earthquake Engineering & Structural Dynamics*, 2020.

[70] F. Alinoori, P. Sharafi, F. Moshiri, and B. Samali, "Experimental investigation on load bearing capacity of full scaled light timber framed wall for mid-rise buildings," *Construction and Building Materials*, vol. 231, p. 117069, 2020.

[71] A. Di Cesare, F. C. Ponzo, N. Lamarucciola, and D. Nigro, "Experimental seismic response of a resilient 3-storey post-tensioned timber framed building with dissipative braces," *Bulletin of Earthquake Engineering*, pp. 1–24, 2020.

[72] H. Bagheri, A. Hashemi, S. Yousef-Beik, P. Zarnani, and P. Quenneville, "New self-centering tension-only brace using resilient slip-friction joint: Experimental tests and numerical analysis," *Journal of Structural Engineering*, vol. 146, no. 10, p. 04020219, 2020.

[73] S. Guo, M. He, Z. Li, F. Liang, F. Chen, Y. Sun, B. Briseghella, and G. He, "Lateral performance of midply wood shear walls with anchor tie-down system: Experimental investigation and numerical simulation," *Construction and Building Materials*, vol. 235, p. 117518, 2020.

[74] I. Lukacs, A. Björnfot, and R. Tomasi, "Strength and stiffness of cross-laminated timber (clt) shear walls: State-of-the-art of analytical approaches," *Engineering Structures*, vol. 178, pp. 136–147, 2019. cited By 14.

7. Acknowledgments

The authors acknowledge the significant contribution of Prof. Roberto Tomasi, who provided us with the experimental data of CLT and LTF shear walls. This work has been supported by the Ministry of Culture of the Czech Republic, research grant NAKI II DG18P02OVV012 - Sustainable Management of Historical Buildings.

8. Appendix

Below the reader can find the Matlab code of the hysteresis model presented in this paper.

```

%% INPUT DATA
%Db1=Positive backbone displacements
%Db2=Negative backbone displacements
%Fb1=Positive backbone forces
%Fb2=Negative backbone forces
%x= Imposed displacement
fr=2;
ns=6;
np=3;
%% OUTPUT DATA
%Fs Simulated Force
%% CODE
for k=2:size(x,1)
if abs(x(k))>abs(x(k-1)) && (x(k))≥max(x(1:k-1)) && x(k)>0 %PHASE 1
[C,I] = min(((x(k)-Db1)).^2);
Fs(k)=Fb1(I);
elseif abs(x(k))>abs(x(k-1)) && (x(k))>min(x(1:k-1))&& x(k)<0 %PHASE 2
[C,I] = min(((min(x(1:k-1))-Db2)).^2);
Fs(k)=((((Fb2(I)+fr)/(abs(min(x(1:k-1))))^np))*(abs(x(k)))^np)-fr;
elseif abs(x(k))<abs(x(k-1))&& x(k)>0 %PHASE 3
TF = islocalmax(Fs(1:k));
F=Fs(1:k);
Fm=vertcat(max(Fs(1:k)),F(TF));
TF = islocalmax(x(1:k));
X=x(1:k);
Xm=vertcat(max(x(1:k)),X(TF));
Fs(k)=((Fm(size(Fm,1))-fr)/((abs(Xm(size(Xm,1))))^ns))*(abs(x(k)))^ns-fr;
elseif abs(x(k))>abs(x(k-1)) && (x(k))≤min(x(1:k-1)) && x(k)<0 %PHASE 4
[C,I] = min(((x(k)-Db2)).^2);
Fs(k)=Fb2(I);
elseif abs(x(k))>abs(x(k-1)) && (x(k))<max(x(1:k-1))&& x(k)>0 %PHASE 5
[C,I] = min(((max(x(1:k-1))-Db1)).^2);
Fs(k)=((((Fb1(I)-fr)/(abs(max(x(1:k-1))))^np))*(abs(x(k)))^np)+fr;
```

```
elseif abs(x(k))<abs(x(k-1))&& x(k)<0 %PHASE 6
TF = islocalmin(Fs(1:k));
F=Fs(1:k);
Fm=vertcat(min(F(1:k)),F(TF));
TF = islocalmin(x(1:k));
X=x(1:k);
Xm=vertcat(min(x(1:k)),X(TF));
Fs(k)=((Fm(size(Fm,1))+fr)/((abs(Xm(size(Xm,1))))^ns))*(abs(x(k)))^ns+fr;
else
Fs(k)=Fs(k-1);
end
end
```

Below the reader can find the Python code of the hysteresis model presented in this paper.

```
# %% Importing libraries, Python version: 3.7.10
# Packages versions:
#     numpy           1.19.5
#     matplotlib      3.4.2
#     scipy           1.7.0
import numpy as np
import matplotlib.pyplot as plt
from scipy.signal import find_peaks

# %% INPUT DATA
# Db1=Positive backbone displacements
# Db2=Negative backbone displacements
# Fb1=Positive backbone forces
# Fb2=Negative backbone forces
# x= Imposed displacement
fr=2
ns=6
n_p=3

# %% OUTPUT DATA
# Fs Simulated Force

# %% CODE
from scipy.signal import find_peaks

for k in range(1,np.shape(x)[0]):
    #PHASE 1
    if abs(x[k])>abs(x[k-1]) and (x[k])>=max(x[:k]) and x[k]>0 :
        C = min(np.power([x[k]-Db1],2))
        I = np.argmin(np.power([x[k]-Db1],2))
        Fs[k]=Fb1[I]
    #PHASE 2
    elif abs(x[k])>abs(x[k-1]) and (x[k])>min(x[:k])and x[k]<0 :
        C = min(np.power(min(x[:k])-Db2,2))
        I = np.argmin(np.power(min(x[:k])-Db2,2))
        Fs[k]=((((Fb2[I]+fr)/(np.power(abs(min(x[:k])),n_p))))
               *np.power(abs(x[k]),n_p))-fr
    #PHASE 3
```

```
        elif abs(x[k])<abs(x[k-1]) and x[k]>0 :
            TF, _ = find_peaks(Fs[:k+1], height=0)
            F  = np.copy(Fs[:k+1])
            Fm = np.hstack((max(Fs[:k+1]),F[TF]))
            TF, _ = find_peaks(x[:k+1], height=0)
            X=np.copy(x[:k+1])
            Xm = np.hstack((max(x[:k+1]),X[TF]))
            Fs[k]=((Fm[np.shape(Fm)[0]-1]-fr)/(np.power(abs(Xm[np.shape(Xm)[0]-1]),ns)))
            *np.power(abs(x[k]),ns)-fr
        #PHASE 4
        elif abs(x[k])>abs(x[k-1]) and (x[k])<=min(x[:k]) and x[k]<0 :
            C = min(np.power(x[k]-Db2,2))
            I = np.argmin(np.power(x[k]-Db2,2))
            Fs[k]=Fb2[I]
        #PHASE 5
        elif abs(x[k])>abs(x[k-1]) and (x[k])<max(x[:k]) and x[k]>0 :
            C = min(np.power([max(x[:k])-Db1],2))
            I = np.argmin(np.power([max(x[:k])-Db1],2))
            Fs[k]=(((Fb1[I]-fr)/np.power(abs(max(x[:k])),n_p))
                    *np.power(abs(x[k]),n_p))+fr
        #PHASE 6
        elif abs(x[k])<abs(x[k-1]) and x[k]<0 :
            TF, _ = find_peaks(-Fs[:k+1], height=0)
            F  = np.copy(Fs[:k+1])
            Fm = np.hstack((min(F[:k+1]),F[TF]))
            TF, _ = find_peaks(-x[:k+1], height=0)
            X=np.copy(x[:k+1])
            Xm=np.hstack((min(x[:k+1]),X[TF]))
            Fs[k]=((Fm[np.shape(Fm)[0]-1]+fr)/(np.power(abs(Xm[np.shape(Xm)[0]-1]),ns)))
            *np.power(abs(x[k]),ns)+fr
        else :
            Fs[k]=Fs[k-1]

# %% Plotting section

figure1 = plt.figure(1)
w=5 # windows width for moving_mean
moving_mean = np.convolve(Fs, np.ones(w), 'same') / w
plt.plot(x,moving_mean,lw=2,ls="dashdot",color="red")
plt.plot(x,Fo,lw=2,color="black")
plt.ylabel('Force [kN]',fontdict=font_labels)
plt.xlabel('Displacement [mm]',fontdict=font_labels)
plt.title('',fontdict=font_titles)
plt.grid(visible=True, which='major', axis='both')
plt.legend(['Sim.','Exp.'],loc="upper left",fontsize=16)
plt.tight_layout()
plt.savefig('CLT_1.png')

figure2 = plt.figure(2)
t = np.arange(0,np.shape(Fo)[0])*0.2
plt.plot(t,moving_mean,lw=2,ls="dashdot",color="red")
plt.plot(t,Fo,lw=2,color="black")
plt.ylabel('Force [kN]',fontdict=font_labels)
plt.xlabel('Time [s]',fontdict=font_labels)
plt.title('',fontdict=font_titles)
plt.grid(visible=True, which='major', axis='both')
plt.legend(['Sim.','Exp.'],loc="upper right",fontsize=16)
plt.tight_layout()
```

```
plt.savefig('CLT_2.png')

E  = np.cumsum(Fo*np.hstack((np.diff(D),0)))
Es = np.cumsum(Fs*np.hstack((np.diff(D),0)))
figure3 = plt.figure(3)
plt.plot(t,Es,lw=2,ls="dashdot",color="red")
plt.plot(t,E,lw=2,color="black")
plt.ylabel('Energy [kJ]',fontdict=font_labels)
plt.xlabel('Time [s]',fontdict=font_labels)
plt.title('',fontdict=font_titles)
plt.grid(visible=True, which='major', axis='both')
plt.legend(['Sim.','Exp.'],loc="upper left",fontsize=16)
plt.tight_layout()
plt.savefig('CLT_3.png')
```